 CMES, vol.13, no.3, pp.219-228, 2006

Stability analysis for inverse heat conduction problems

Xianwu Ling[1], **S.N. Atluri**[1]

Abstract: In this paper, two matrix algebraic tools are provided for studying the solution-stabilities of inverse heat conduction problems. The propagations of the computed temperature errors, as caused by a noise in temperature measurement, are presented. The spectral norm analysis reflects the effect of the computational time steps, the sensor locations and the number of future temperatures on the computed error levels. The Frobenius norm analysis manifests the dynamic propagations of the computed errors. As an application of the norm analysis, we propose a method for the best positioning of the thermocouples.

1 Introduction

The inverse heat conduction problem (IHTP) consists in the estimation of the surface heat flux history, given one or more interior measured temperatures. The IHCP is much more difficult to solve than the direct heat conduction problem in which the initial and boundary conditions are given and the temperatures are to be determined. Unlike the direct problem wherein the high frequency components of the heat fluxes are damped out due to the diffusive nature of the heat conduction process, the opposite takes place in the IHCP. The high frequency components or noise in the temperature measurements will be amplified in the projection to the surface and lead to oscillations in the computed surface fluxes.

There have been varied approaches to the inverse heat conduction problem. In terms of methodology, these have included the exact solution technique [Burggraf (1964)], the inversion of Duhamel's integral [Stolz (1960), Beck (1968)], Laplace transformation techniques [Sparrow (1964), Imber (1972)], the control volume method [Taler (1996)], the use of Helmholtz equation [Grysa (1989)], the finite difference method [Beck (1965, 1970, 1981, 1982), Blackwell (1981), Hensel (1984)], the finite element approaches [Hore (1977), Bass (1980), Ling et al. (2003, 2005)], the digital filtering method [Hills (1986), Hensel (1986)], the eigenvalue reduction method [Tandy (1986)], the group preserving scheme [Chang et al. (2005)], Tikhonov regularization method [Tikhonov (1977)], Alifannov iterative regularization [Alifannov (1994)], the mollification method [Murio (1993)], the hyperbolic regularizaiton method [Weber (1981)], the conjugate gradient method [Özisik and Orlande (2000)] and the dynamic programming technique [Trujillo and Busby (1997)], among many others.

As the IHCP finds wide applications in quenching and many other thermal-related industries, it is of great practical importance to study the various effects on the stability of the inverse solutions. Surprisingly, despite so many existing inverse techniques, to the best knowledge of the authors, a systematic study of the stability of the inverse solutions has not been pursued. Most of the techniques do not give a quantitative method for determining the computed errors due to noise in temperature measurements. The reason for a lack of studies on the stability of the solution of the inverse problem is simple. The IHCP is already very difficult, its solution instability analysis is even more. Very limited stability analysis can be found in Murio (1983), Beck and Blackwell (1985) and Maciag and Al-Khatib (2000). The fact is that, however, inverse solutions are extremely sensitive to measurement errors, measurement locations, and computational step times. A small temporal noise in the interior measurements tends to produce large oscillations in the surface boundary condition estimation, which becomes even more significant as the sensors are placed farther away from the surface heat fluxes. In addition, contrary to the direct problem, the use of smaller time steps can introduce instabilities in the inverse solutions. Therefore, a large computational time step is often used in the IHCP, which can lead to a poor resolution of the results.

The present work aims to systematically investigate the stability of the inverse solutions. Two matrix norm tools are provided for measuring the instability of the inverse solutions. The effects of measurement locations, the

[1] Center for Aerospace Research and Education,
University of California at Irvine
5251 California Ave., Suite 140, Irvine, CA 92612

computational time steps, and the number of future temperatures on the error propagation are studied. Also, using the norm analysis tools, we endeavor to answer a common question confronting many thermal engineers when designing heat transfer experiments, i.e., where are the best locations to put the thermocouple? This poses a very important issue in inverse heat conduction problems, as poorly positioned sensors inevitably lead to a poor inverse solution. The problem becomes even serious when a complex shaped object, subjected to multiple surface heat fluxes, has to be considered. Our analysis in this work, to the best knowledge of the authors, for the first time provides a unique and systematic answer to the question.

2 Theoretical development

In this section, a brief overview is first made of the inverse algorithm proposed in Ling et al. (2006). Second, we derive the propagation equations of the measured temperature errors. And last, we provide two matrix norm analyses that can be used to monitor the error propagations.

The inverse problem is stated as follows Ling et al. (2006): for a region subjected to the first kind (Γ_1) and the second kind (Γ_2) of boundary conditions, given the temperature measurements Y_m^ι at $m = 1,2,\ldots,M$ interior sites and $\iota = 1,2,\ldots,I$ experimental times, determine the unknown surface heat fluxes q_j^i at $j = 1,2,\ldots,J$ discretized nodes on Γ_2 for $i = 1,2,\ldots,I$ computational times. Note that it is required that $J \leq M$ in order to ensure a solution, and often that $I \leq I$ in order to ensure a convergent solution.

The inverse solutions of q_j^{i+1} are obtained by minimizing the square error norm s^{i+1} between the measured and the calculated temperatures summed over $r = 0,1,\cdots,R$ future time steps for each computational time i, i.e.,

$$s^{i+1} = \sum_{m=1}^{M}\sum_{r=0}^{R}\left(Y_m^{(r)} - \tilde{\theta}_m^{(r)}\right)^2 + \sum_{p=1}^{P}\sum_{j=1}^{J} w_j^{(-p)}\left(q_j^{(-p)} - q_j^{i+1}\right)^2, \tag{1}$$

where the superscript $(.)$ indicates the time index that is measured with respect to the *current* time i (not the *initial* one). Note that the past heat fluxes $q_j^{(-p)}$ are added in the same sense as the Tikhonov regularization [Tikhonov (1977)]. $\tilde{\theta}_m^{(r)}$ is the component of the calculated temperature vector $\tilde{\theta}^{(r)}$ at the measurement site m and the future time (r). $\tilde{\theta}^{(r)}$ is a subset of the global temperature vector $\theta^{(r)}$, which is a function of the unknown heat fluxes $\mathbf{q}^{i+1}$.

In order to solve for $\theta^{(r)}$, we employ the explicit heat conduction equation

$$\left(\mathbf{M} + \Delta t^{(r)}\mathbf{K}\right)\theta^{(r)} = \mathbf{M}\theta^i + \Delta t^{(r)}\mathbf{f}^{(r)} + \mathbf{c}^{(r)}, \tag{2}$$

where $\Delta t^{(r)} = t^{(r)} - t^i = \Delta t + r\Delta\tau$, and where Δt is the inverse computational time-step and $\Delta\tau$ is the experimental time-step. The last term $\mathbf{c}^{(r)}$ on the righthand side of equation (2) comes from the condensation of the temperatures on Γ_1. The heat flux force $\mathbf{f}^{(r)}$ can be linearly related to $\mathbf{q}^{i+1}$ via the FEM discretization, i.e.,

$$\mathbf{f}^{(r)} = \mathbf{D}\mathbf{q}^{i+1}, \tag{3}$$

where $\mathbf{D}$ is a constant matrix.

Inverting equation (2) gives

$$\theta^{(r)} = \mathbf{G}^{(r)}\theta^i + \mathbf{X}^{(r)}\mathbf{q}^{i+1} + \mathbf{d}^{(r)}, \tag{4}$$

where

$$\mathbf{G}^{(r)} = U^{(r)}\mathbf{M}, \text{ and } U^{(r)} = \left[\mathbf{M} + \Delta t^{(r)}\mathbf{K}\right]^{-1}, \tag{5}$$

and where

$$\mathbf{X}^{(r)} = \frac{\partial\theta^{(r)}}{\partial\mathbf{q}^{i+1}} = \Delta t^{(r)}\mathbf{U}^{(r)}\mathbf{D}, \tag{6}$$

is the generalized sensitivity matrix. Now, $\tilde{\theta}^{(r)}$ can be obtained by mapping the local index m to the global node m such that $\tilde{\theta}_m^{(r)} = \theta_{\mathsf{m}}^{(r)}$, which yields

$$\tilde{\theta}^{(r)} = \tilde{\mathbf{G}}^{(r)}\theta^i + \tilde{\mathbf{X}}^{(r)}\mathbf{q}^{i+1} + \tilde{\mathbf{d}}^{(r)}, \tag{7}$$

where $\tilde{G}_{mn}^{(r)} = G_{\mathsf{mn}}^{(r)}$ and where $\tilde{X}_{mj}^{(r)} = X_{\mathsf{m}j}^{(r)}$ is the sensitivity coefficient at the measurement site m with respect to the surface flux j at the future time (r).

Minimization of s^{i+1} (with respect to $\mathbf{q}^{i+1}$) leads to the governing equation for the inverse problem, which in the matrix form is written as

$$\left(\sum_{r=0}^{R}\left[\tilde{\mathbf{X}}^{(r)}\right]^T\tilde{\mathbf{X}}^{(r)} + \sum_{p=1}^{P}\mathbf{w}^{(-p)}\right)\mathbf{q}^{i+1} = \sum_{r=0}^{R}\left[\tilde{\mathbf{X}}^{(r)}\right]^T\left(\mathbf{Y}^{(r)} - \hat{\theta}^{(r)}\right) + \sum_{p=1}^{P}\mathbf{w}^{(-p)}\mathbf{q}^{(-p)}, \tag{8}$$

where $\hat{\theta}^{(r)}$ is the temperature at the measurement sites for *zero* heat flux $\mathbf{q}^{i+1}$, which, from equation (7), is given as

$$\hat{\theta}^{(r)} = \tilde{\mathbf{G}}^{(r)}\theta^i + \tilde{\mathbf{d}}^{(r)}. \tag{9}$$

As emphasized by Ling et al. (2006), formula (8) represents a generic system of equations regardless of the underlying numerical methods, although it was developed based on the finite element method (FEM). Interested readers are referred to Ling et al. (2006) for detailed developments of the algorithm. We mention that the most expensive part in solving equation (8) is the calculations of the sensitivity coefficient matrix $\tilde{\mathbf{X}}^{(r)}$. Various methods can been employed in calculating the sensitivity coefficients, such as the analytical method [Burggraf (1964)], the finite different method [Beck (1965, 1970, 1981, 1982)], the finite element method [Ling et al. (2003, 2005)], the boundary element method [Divo et al. (2004)], and the meshless method [Sladek et al. (2005)], to mention only a few.

For many industrial materials, the thermal properties (namely the conductivity, the capacity and the density) do not change much with temperatures. Hence, we focus below on the instability analysis for the linear heat conduction problem in which case $\tilde{\mathbf{X}}^{(r)}$ do not change with the temperature. The nonlinear problem can be studied likewise in a step by step manner. Without loss of generality, we further suppose that there exists only one set of measurement error $\delta\mathbf{Y}^1$ in $\mathbf{Y}^1$, and that all the subsequent temperature measurements are error free, i.e., $\delta\mathbf{Y}^i = \mathbf{0}$ for $i = 2,3,\cdots$. Such a supposition is to reveal the characteristics of the error propagation, because multiple errors in subsequent time add only the complexity but not the difficulty to the analysis.

For simplicity, the past heat regularization is deactivated by setting $w_j^{(-p)} = 0$. Hence, equation (8) yields

$$\left(\sum_{r=0}^{R}\left[\tilde{\mathbf{X}}^{(r)}\right]^T\tilde{\mathbf{X}}^{(r)}\right)\delta\mathbf{q}^{i+1} = -\sum_{r=0}^{R}\left[\tilde{\mathbf{X}}^{(r)}\right]^T\delta\hat{\theta}^{(r)} \quad \text{for } i = 1,2,\cdots. \tag{10}$$

We assume that the temperatures can be measured accurately on Γ_1, i.e. $\delta\tilde{\mathbf{d}}^{(r)} = \mathbf{0}$. From equation (9), one obtains

$$\delta\hat{\theta}^{(r)} = \tilde{\mathbf{G}}^{(r)}\delta\theta^i, \tag{11}$$

which, upon plugging into equation (10), gives

$$\delta\mathbf{q}^{i+1} = -\left(\sum_{r=0}^{R}\left[\tilde{\mathbf{X}}^{(r)}\right]^T\tilde{\mathbf{X}}^{(r)}\right)^{-1}\left(\sum_{r=0}^{R}\left[\tilde{\mathbf{X}}^{(r)}\right]^T\tilde{\mathbf{G}}^{(r)}\right)\delta\theta^i, \tag{12}$$

for $i = 1,2,\cdots$. To see how the calculated temperature errors propagate, from equation (4), we obtain

$$\delta\theta^{i+1} = \mathbf{G}^{(0)}\delta\theta^i + \mathbf{X}^{(0)}\delta\mathbf{q}^{i+1}. \tag{13}$$

Upon substituting equation (12) into equation (13), it renders

$$\delta\theta^{i+1} = \mathbf{E}\delta\theta^i, \text{ for } i = 1,2,\cdots \tag{14}$$

where the error propagate matrix $\mathbf{E}$ is defined as

$$\mathbf{E} = \mathbf{G}^{(0)} - \mathbf{X}^0\left(\sum_{r=0}^{R}\left[\tilde{\mathbf{X}}^{(r)}\right]^T\tilde{\mathbf{X}}^{(r)}\right)^{-1}\left(\sum_{r=0}^{R}\left[\tilde{\mathbf{X}}^{(r)}\right]^T\tilde{\mathbf{G}}^{(r)}\right) \tag{15}$$

for $i = 1,2,\cdots$.

The effect of the initial temperature errors on the predicted heat fluxes is also an important subject, but it can be studied using the same method as proposed in the current work. Hence, we assume here that the initial temperatures are error free, i.e., $\delta\theta^0 = \mathbf{0}$, so that we can focus on the propagation of $\delta\mathbf{Y}^1$ with time. For the first time step (i.e., $i = 0$), the temperature error propagation needs a separate treatment as follows. With $\delta\theta^0 = \mathbf{0}$, equation (4) yields

$$\delta\theta^1 = \mathbf{X}^{(0)}\delta\mathbf{q}^1. \tag{16}$$

In order to derive $\delta\mathbf{q}^1$, we use the supposition that $\delta\mathbf{Y}^i = \mathbf{0}$ for $i = 2,3,\cdots$, and that $\delta\theta^0 = \mathbf{0}$. Then, equation (8) gives

$$\left(\sum_{r=0}^{R}\left[\tilde{\mathbf{X}}^{(r)}\right]^T\tilde{\mathbf{X}}^{(r)}\right)\delta\mathbf{q}^1 = \sum_{r=0}^{R}\left[\tilde{\mathbf{X}}^{(r)}\right]^T\left(\delta\mathbf{Y}^{(r)} - \delta\hat{\theta}^{(r)}\right), = \left[\tilde{\mathbf{X}}^{(0)}\right]^T\delta\mathbf{Y}^1,$$

i.e.,

$$\delta\mathbf{q}^1 = \left(\sum_{r=0}^{R}\left[\tilde{\mathbf{X}}^{(r)}\right]^T\tilde{\mathbf{X}}^{(r)}\right)^{-1}\left[\tilde{\mathbf{X}}^{(0)}\right]^T\delta\mathbf{Y}^1. \tag{17}$$

Hence, equations (16) and (17) give

$$\delta\theta^1 = \mathbf{A}\delta\mathbf{Y}^1, \tag{18}$$

where

$$\mathbf{A} = \mathbf{X}^{(0)} \left(\sum_{r=0}^{R} \left[\tilde{\mathbf{X}}^{(r)}\right]^T \tilde{\mathbf{X}}^{(r)} \right)^{-1} \left[\tilde{\mathbf{X}}^{(0)}\right]^T \quad \text{for } i = 0, \tag{19}$$

indicates the initial error propagation matrix.

Equations (14) and (18) provide the mathematical foundation for analyzing the error propagation of $\delta\mathbf{Y}^1$. To see this, we express the calculated temperature errors at $i+1$ step that is due to $\delta\mathbf{Y}^1$ as

$$\delta\theta^{i+1} = (\mathbf{E})^i \mathbf{A}\delta\mathbf{Y}^1. \tag{20}$$

Note that $\mathbf{E}$ is raised to the power of i for the $(i+1)^{th}$ time step.

To ensure that $\|\delta\theta^{i+1}\|$ remain bounded as i increases, it is required that the spectral norm of $\mathbf{E}$ be less than 1 [c.f., Burden (1985)]. The spectral norm of a matrix is defined as

$$\|\mathbf{E}\|_s = \sqrt{\lambda_{max}(\mathbf{E}^H \cdot \mathbf{E})} \tag{21}$$

where $\mathbf{E}^H$ stands for the conjugate transpose of $\mathbf{E}$, where λ_{max} denotes extracting the maximum eigenvalue of $\mathbf{E}^H \cdot \mathbf{E}$. Since $\mathbf{E}$ is a real number matrix, $\mathbf{E}^H = \mathbf{E}^T$.

The spectral norm $\|\mathbf{E}\|_s$ provides a useful tool for analyzing the effect of the various factors such as R, Δt and measurement sites on the stability of the inverse solution, but it does not reveal how $\delta\mathbf{Y}^1$ propagate with time. To this end, we define

$$\omega^{i+1} = \frac{\|\delta\theta^{i+1}\|}{\|\delta\mathbf{Y}^1\|} = \|(\mathbf{E})^i \mathbf{A}\|, \tag{22}$$

by taking the norm of equation (20). Hence, ω^{i+1} reflects the dynamic propagation of a unit measurement error in $\mathbf{Y}^1$. Apparently, the smaller ω^{i+1} is, the larger the error is suppressed. Several forms of matrix norms are available, but it is expected that they perform equally effective in examining the error propagations. We select for our analysis the Frobenius norm, which is defined as the square root of the summation of the matrix element squares, i.e.,

$$\omega^{i+1} = \|\mathbf{E}^i\mathbf{A}\| = \sqrt{\sum_{row=1}\sum_{col=1}\left[(\mathbf{E}^i\mathbf{A})_{row,col}\right]^2}. \tag{23}$$

Like the spectral norm analysis, the inverse solution is convergent on the condition that $\omega^{i+1} < 1$. The predicted surface heat flux error $\delta\mathbf{q}^{i+1}$ due to $\delta\mathbf{Y}^1$ can be similarly analyzed using equations (12) and (17), but this analysis do not provide anything newer than that already embodied in $\|\mathbf{E}\|_s$ and ω^{i+1} (which point is validated by our numerical tests). Hence, in the next section, we only present results of $\delta\mathbf{Y}^1$ on $\delta\theta^{i+1}$.

3 Numerical tests

In this section, we study two example problems using the spectral norm and the Frobenius norm analyses. Also, we demonstrate that the stability analysis provides a tool for inversely designing the quenching experiment.

In the first example problem, a flat plate of unit length is insulated at $\overline{x} = 0$ and exposed to a heat flux q at $L = \overline{x} = 1$, where $\overline{x}$ indicates the dimensionless distance from the insulated end. Only one sensor is supposed to be located at $\overline{x} = 0, 0.5$ and 0.9, respectively. The thermal conductivity $k = 1$, the thermal capacity $c = 1$ and the density $\rho = 1$. We choose the experimental time step as $\Delta\tau = 0.01L^2/\alpha$, where $\alpha = \rho c/k$ is the thermal diffusion coefficient. Hence, $\Delta\tau$ is 1% of the characteristic diffusion time of the plate. The computational time-step Δt is an integer multiple of the experimental time-step, namely, $\Delta t = n\Delta\tau$, where n represents the sampling rate.

Figure 1 shows the variation of the spectral norms with the time steps (Δt), the number of future temperatures (R) and the measurement locations ($\overline{x}$). It is seen that that for $\overline{x} = 0$ (i.e. the sensor is placed at the opposite end to the flux), very large errors are expected, while for $\overline{x} = 0.9$ (i.e. the sensor is put very close to the flux), very small errors are rendered. The error levels for $\overline{x} = 0.5$ are between those of $\overline{x} = 0$ and $\overline{x} = 0.9$. The effect of using future temperatures depends much on the sensor locations. When the sensor is far from the surface, the number of future temperatures has a significant role in suppressing the error propagations. On the contrary, when the sensor is close to the surface, the effect of using future temperature is diminished. In passing, we also note that there exists a critical time step for a fixed sensor location $\overline{x}$ and a chosen number of future temperatures (R). This is illustrated for $\overline{x} = 0$ in Figure 1(a), from which it can be read that $\Delta t_{cri} = 0.38$ for $R = 0$ and $\Delta t_{cri} = 0.27$ for $R = 8$. For $\overline{x} = 0.9$ as shown in Figure 1(c), no such critical time step exists, because $\|\mathbf{E}\|_s$ is always lower than the unity. We will show below that the critical time step thus obtained

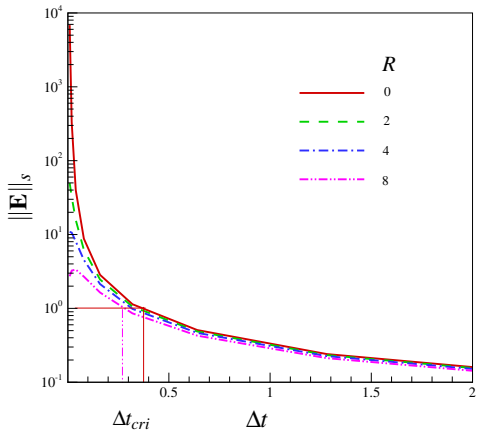

(a) $\overline{x} = 0$

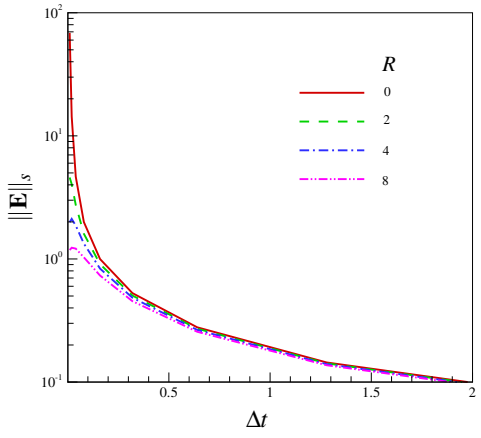

(b) $\overline{x} = 0.5$

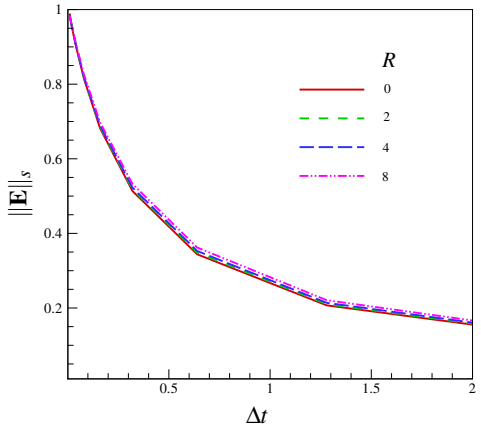

(c) $\overline{x} = 0.9$

Figure 1 : The spectral norm for the 1D planar problem.

can be used to predesign the temperature measurement sites for a quenching part of complex shape.

Now we demonstrate the dynamic propagation of the calculated temperature errors. Figure 2 shows the variation of ω^{i+1} for $\overline{x} = 0$. Figure 2 illustrates the dramatic effect of computational time step (represented by n) and the number of the future temperatures (R). Not surprisingly, ω^{i+1} decreases with increasing n and R. It is worth mentioning that increasing n is at the cost of a poor resolution of the result, hence often undesirable. We observe from 2(b) that for a large $R = 8$, the initial errors are even smaller for a small n than for a large n, although the overall error suppression rates are much larger in the latter case. In Figure 3, the variations of ω^{i+1} are shown for $\overline{x} = 0.9$. Needless to say, a sensor closer to the surface greatly reduces the error levels. Again the initial errors are smaller for a small n than for a large n when a large R is employed. The significance of this interesting observation is that for a large R, a small computational time step can be used not only to improve the resolution, but to improve the accuracy. Although this observation appears at the first glance to violate one's intuition, it exactly indicates the dramatic effect of using future temperatures. Although we do not show the results here, we would like to mention two additional observations: (1) regarding the number of elements that should be used in the 1D problem, our simulations indicate that twenty elements along the line are sufficient, because further increasing the number of elements changes very slightly the error levels and their propagation rates; (2) we also perform the stability analysis for 1D axisymmetric problem. Under the same parameters, it is found that the axisymmetric problem is less sensitive to the measurement errors than the 1D planar problem, hence a smaller computational time-step can be used.

Our 2D planar problem follows that in Ling et al. (2006) and Tandy et al. (1986). A 2D slab, as discretized in Figure 4, is subjected two fluxes on the top and the left surfaces. Again, we choose $\Delta\tau = 0.01L^2/\alpha$, where L is the length of the slab. We first investigate the error propagation when the temperature measurements are taken at nodes 11 and 23. Figure 5 shows the variation of the spectral norm versus the computational time step Δt. The number of future temperature (R) is seen to dramatically affect the error levels; or alternatively speaking, Δt_{cri} is much smaller for a large R, e.g., $\Delta t_{cri} = 0.07$ for $R = 8$ while $\Delta t_{cri} = 0.14$ for $R = 0$. Figure 6 shows the dy-

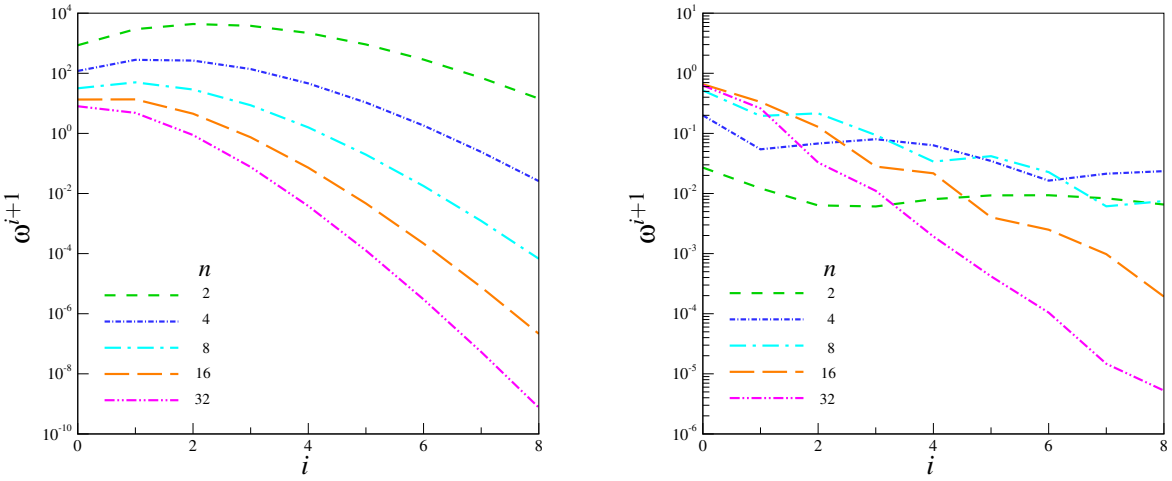

(a) $R = 0$ (b) $R = 8$

Figure 2 : The dynamic error propagation for 1D planar problem. $\overline{x} = 0$.

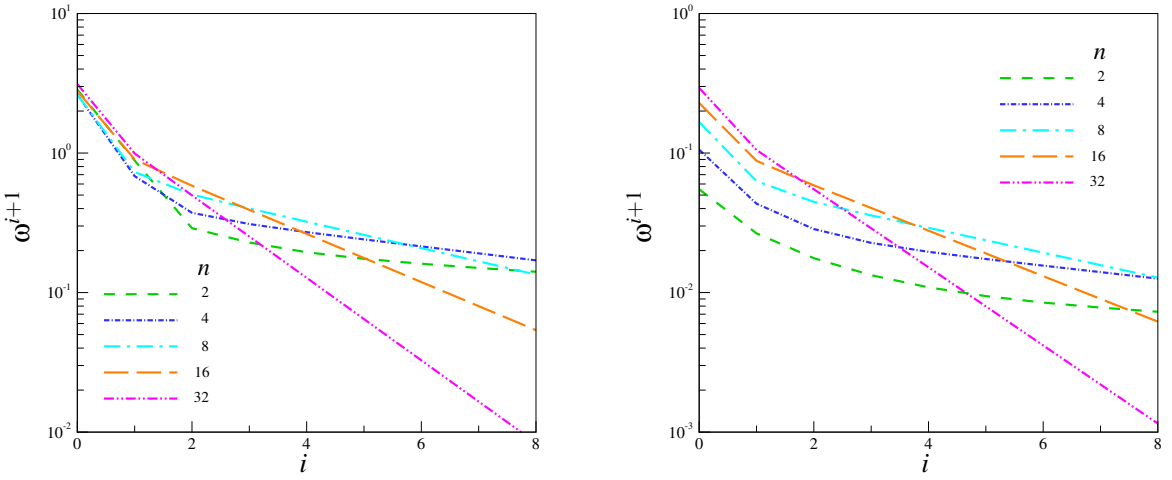

(a) $R = 0$ (b) $R = 8$

Figure 3 : The dynamic error propagation for 1D planar problem. $\overline{x} = 0.9$.

namic error propagations when the measurement sites are at nodes 11 and 23. A comparison of Figure 6 (a) and (b) indicates that using future temperatures effects via significantly reducing the initial error levels, not the overall error suppression rates. Surprisingly, the error suppression rates are even smaller for a large R than for a small R. Again, from Figure 6(b), in order to improve solution resolution, we suggest that a small sampling rate n be used for a large R.

As mentioned in the Introduction, a common difficulty that confronts many thermal engineers in designing heat transfer experiments is where to best put the thermocouple. For instance, this is a universal issue in the quenching industry. Here, we reinterpret 'best' in the sense that the inverse solution is the least polluted when subjected to noise in temperature measurements. From Figure 1(a), we see that the error level is directly related and inversely proportional to the critical time step $\Delta\tau_{cri}$. This is a general observation, not limited to the dimensions of the problem and regardless of the parameters used (e.g., R, n, etc). Hence, we can turn to the spectral norm for help, and use $\Delta\tau_{cri}$ as an indicator as the error level. In the

Table 1 : The first ten smallest $\Delta\tau_{cri}$'s (in the unit of 10^{-1}). $\Delta\tau = 0.01L^2/\alpha$.

$R=0$		$R=2$		$R=4$		$R=8$	
pair	$\Delta\tau_{cri}$	pair	$\Delta\tau_{cri}$	pair	$\Delta\tau_{cri}$	pair	$\Delta\tau_{cri}$
[6,13]	0.454060	[8,14]	0.125000	[8,14]	0.125000	[8,14]	0.125000
[9,14]	0.458443	[6,13]	0.125000	[6,13]	0.125000	[6,13]	0.125000
[6,19]	0.458968	[9,14]	0.142124	[6,19]	0.125000	[7,12]	0.125000
[7,13]	0.460591	[7,13]	0.149076	[7,19]	0.125000	[7,11]	0.125000
[6,14]	0.465702	[7,14]	0.159297	[6,14]	0.125000	[7,14]	0.125000
[8,14]	0.474371	[6,14]	0.166226	[9,14]	0.125000	[7,13]	0.125000
[7,14]	0.477972	[6,19]	0.183410	[7,14]	0.125000	[6,12]	0.125000
[7,19]	0.478605	[7,19]	0.225730	[7,13]	0.125000	[6,11]	0.125000
[8,13]	0.493062	[8,13]	0.326609	[6,12]	0.126066	[8,19]	0.125000
[6,18]	0.553461	[8,19]	0.349251	[8,19]	0.140524	[6,24]	0.125000

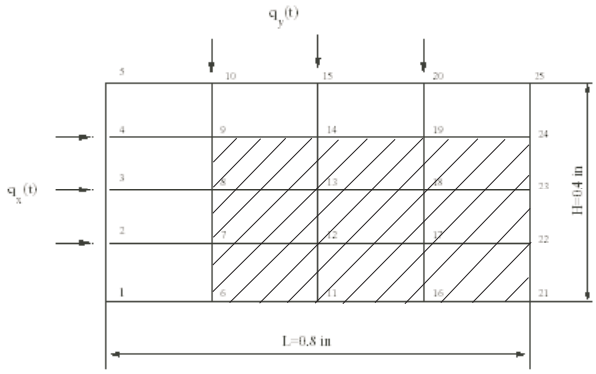

Figure 4 : FEA model of the 2D slab with two unknown fluxes.

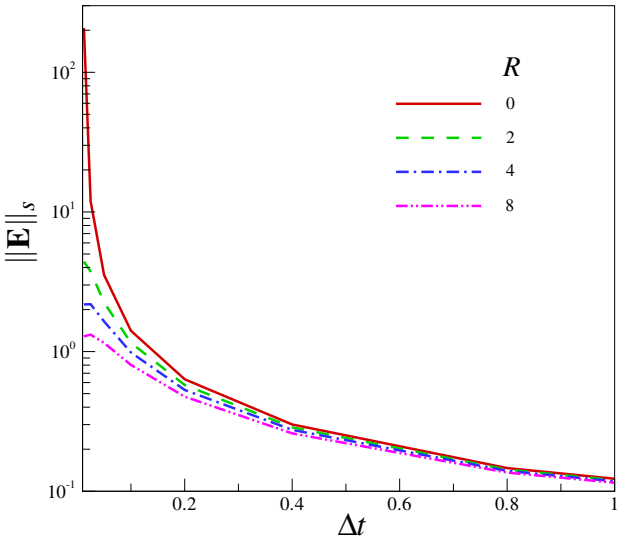

Figure 5 : The spectral norm for the 2D planar problem when the measurement sites are at nodes 11 and 23.

following, we illustrate the concept using the 2D planar problem as shown in Figure 4. Suppose that the top and the left surfaces are inaccessible, so that we limit ourselves in the shadow region for selecting a pair of nodes, such as [11,23], to put the sensor. Now, we ask: which pair would give the best solution? To address the question, we perform a loop search for each possible pair of nodes in the shadow region and calculate $\Delta\tau_{cri}$. Table 1 shows the calculations for the first ten smallest $\Delta\tau_{cri}$'s for $\Delta\tau = 0.01L^2/\alpha$. Table 1 demonstrates several very interesting points: (1) the 'best' measurement locations is relative to R. For instance, for $R=0$, the best locations are given by [6,13], while for $R=2$, [6,13] and [8,14] are equally effective; (2) when many future temperatures are used, the 'best' measurement location become vaguely defined, since many pairs produce the same $\Delta\tau_{cri}$'s. Actually, for $R=8$, the first thirty smallest $\Delta\tau_{cri}$'s are all equal (not shown in the Table 1). This means that, with a large R, the specific measurement locations are not that important (which is good news indeed). However, we need to point out that the second observation is not general, because in extracting $\Delta\tau_{cri}$ for a given large R, if the largest $\|\mathbf{E}\|_s$ for a pair is already smaller than the unity, we merely set $\Delta\tau_{cri}$ to the experimental time-step $\Delta\tau$. For instance, when $R=8$, $\Delta\tau_{cri}$ is found to equal $\Delta\tau$ for the first thirty node pairs. Hence, the definition of the best 'pair' is related to the experimental time-step $\Delta\tau$.

In Ling et al. (2005, 2006), we suggest that the exper-

Table 2 : The first ten smallest $\Delta\tau_{cri}$'s (in the unit of 10^{-1}). $\Delta\tau = 0.002L^2/\alpha$.

$R=0$		$R=2$		$R=4$		$R=8$		$R=10$	
pair	$\Delta\tau_{cri}$	pair	$\Delta\tau_{cri}$	pair	$\Delta\tau_{cri}$	pair	$\Delta\tau_{cri}$	pair	$\Delta\tau_{cri}$
[6,13]	0.436186	[6,13]	0.384095	[6,13]	0.346718	[6,13]	0.223304	[8,14]	0.028748
[9,14]	0.437953	[9,14]	0.387741	[7,13]	0.354928	[7,13]	0.235320	[6,13]	0.156123
[7,13]	0.447697	[7,13]	0.388714	[9,14]	0.356221	[9,14]	0.236814	[9,14]	0.163195
[6,19]	0.450539	[6,19]	0.390682	[6,19]	0.358988	[8,14]	0.248898	[7,13]	0.165496
[6,14]	0.469183	[6,14]	0.396105	[6,14]	0.366887	[6,19]	0.258524	[6,14]	0.195470

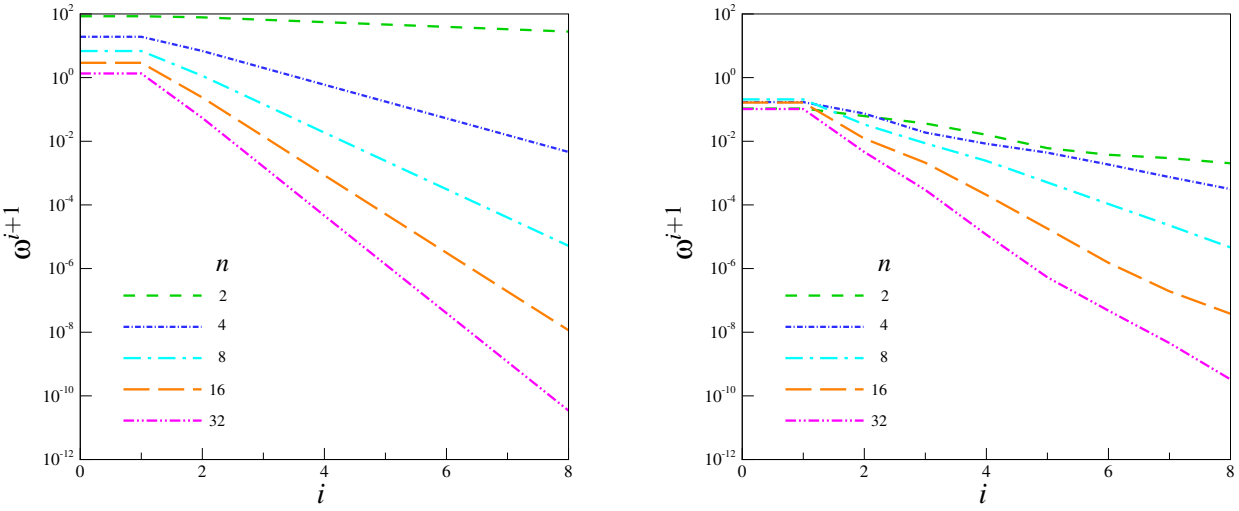

(a) $R=0$ (b) $R=8$

Figure 6 : The dynamic error propagation for 2D planar problem.

imental time-step $\Delta\tau$ be set to the smallest value of the reading intervals allowed in the thermal control unit, so that the maximal information can be used. This suggestion is also valid in determining the best locations for the thermocouple. In Table 2, we show the first five smallest $\Delta\tau_{cri}$'s for $\Delta\tau = 0.002L^2/\alpha$. We see that a small $\Delta\tau$ not only sharpens the distinction of the best sensor locations, but also decreases the smallest $\Delta\tau_{cri}$ that can be used (thus improving the resolution). Comparing the smallest Δt_{cri} for $R=8$ and $R=10$ in Table 2, Δt_{cri} is seen to be dramatically decreased. One point that needs explanation when comparing Table 1 and Table 2 is that when $R=8$, why is the smallest $\Delta\tau_{cri}$ even larger for $\Delta\tau = 0.002L^2/\alpha$ than for $\Delta\tau = 0.01L^2/\alpha$? This is due to the way that the future temperatures are used, i.e., the future temperatures are extracted at each and every experimental time steps. The period of the future time is given by $R\Delta\tau$. Obviously, much less future temperatures are used in the case of $\Delta\tau = 0.002L^2/\alpha$ than that of $\Delta\tau = 0.01L^2/\alpha$. As less future temperatures are used in the case of $\Delta\tau = 0.002L^2/\alpha$, a larger $\Delta\tau_{cri}$ is needed.

The smallest experimental reading interval $\Delta\tau$ may well be physically limited by the thermal control unit. If one has to select a pair that gives the 'best' measurement location among the pairs that generate the equally smallest $\Delta\tau_{cri}$'s, two additional principles are suggested: (1) select the pair that has the lowest ω^{i+1} in magnitudes using the Frobenius analysis. To illustrate the point, we see that from Table 1, the smallest $\Delta\tau_{cri}$'s are indistinguishable for $R=2$ between the measurement locations [8,14] and [6,13]. Figure 7 shows the Frobenius norms for the two pairs. A comparison of the Frobenius norms indicates that for $R=0$, [6,13] obviously outperforms than [8,14], but for $R=2$, [8,14] is slight better a choice than [6,13] (because the Frobenius norm is slight smaller for [8,14]); (2) to prevent interference among the sensors, the pair

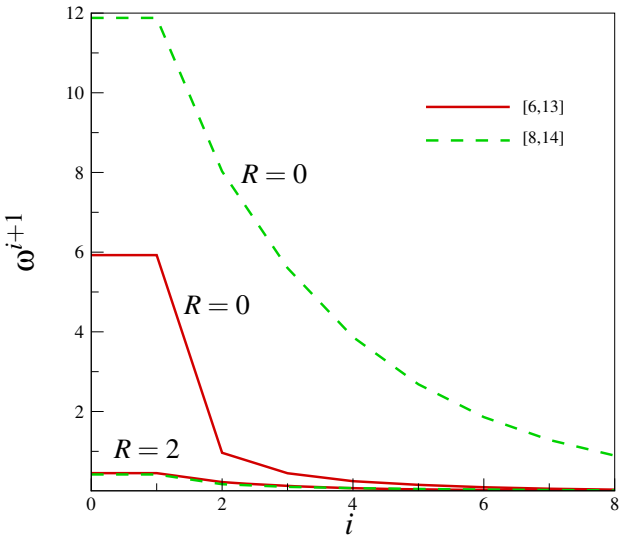

Figure 7 : A comparison of the Frobenius norms for [6,13] and [8,14]. $\Delta\tau = 0.01L^2/\alpha$.

sensors should be put as far away as possible. The interference among the sensors is not considered here, but is expected to affect to a large degree the accuracy of the inverse solution. Finally, we mention that a brute-force loop from node to node is used in the current search of the best pair of measurement locations. In a small scale problem, such as the current 2D planar model, the brute-force search scheme is computationally affordable. But for a problem of a large scale (say, with thousands of nodes), a better search scheme is needed. This will be reported in our forthcoming work.

4 Summary

In summary, the present work provides a method to analyze the error propagations in the inverse heat conduction problems, and ways to best position the sensors in heat conduction experiments. To the best knowledge of the authors, our work appears to be the first one that systematically looked into stability issues in the IHCP and the first one that provides a theoretical guidance for the "best" placement of the thermocouple.

The spectral matrix norm can provide a static analysis of the effect of the various factors on the error level, such as the computational time-step, the number of future temperatures, and the locations of the thermocouple, while the Frobenium matrix norm provides a dynamic propagation of the computed errors. Two example problems are given to test the proposed method. The number of future temperatures is found to dramatically affect the level of the computed errors and the rate of their propagations. It is suggested that a small sampling rate is used together with a large number of future temperatures. For the 1D planar and axisymmetric problems, twenty finite elements are sufficient for the IHCP. The axisymmetric 1D problem is less sensitive to the measurement errors than the 1D planar problem, thus a smaller computational time-step can be used.

Finally, this stability analysis can also be used in the inverse design of the quenching experiment. By selecting the smallest Δt_{cri}, it becomes possible to locate the best thermocouple positions, so that measurement errors have the least effect on the inverse solutions. Again, a large number of future temperatures can reduce the sensitivity of the calculated surface fluxes to the choice of the measurement locations.

Acknowledgement: This work is supported by the Army Research Laboratory. The first author would also thank Dr. H.P. Cherukuri for supporting his PhD work, during which period part of the ideas in the present work was brewed.

References

Alifannov O.M. (1994): Inverse heat transfer problems, Springer-Verlag, New York.

Bass B. (1980): Application of the finite element method to the nonlinear inverse heat conductin problem using Beck's second method, *Transaction of ASME*, vol. 102, pp. 168-176.

Beck J.V. (1968): Surface heat flux determination using an integral method, *Nucl. Eng. Des.*, vol. 7, pp. 170-178.

Beck J.V., and Wolf H. (1965): The nonlinear inverse heat conduction problem, *ASME paper*, No. 65-HT-40.

Beck J.V. (1970): Nonlinear estimation applied to nonlinear inverse heat conduction problem. *Int. J. heat Mass Transfer*, vol. 13, pp. 703-716.

Beck J.V. (1981): Review of six inverse heat conduction computer codes. ANL/RAS/LWR 81-1, Argonne National Laboratory, Argonne.

Beck J.V., Blackwell B., and St. Clair C.R. (1985): Inverse Heat Conduction: Ill-Posed Problems, Wiley Interscience, New York.

Beck J.V., Litkouhi B., and St. Clair C.R. (1992): Efficient sequential solution of the nonlinear inverse heat conduction problem, *Numerical Heat Transfer*, vol. 5, pp. 275-286.

Blackwell B.F. (1981): Efficient technique for the numerical solution of the one-dimensonal inverse problem of heat conduction, *Numerical Heat Transfer*, vol. 4, pp. 229-238.

Burden R.L., and Faires J.D. (1985): Numerical Analysis, Prindle, Weber& Schmidt.

Burgrraf O.R. (1964): An exact solution of the inverse problem in heat conduction theory and applications, *J. Heat Transfer*, vol. 86C, pp. 373-382.

Chang C.W., Liu C.S., and Chang J.R. (2005): A group preserving scheme for inverse heat conduction problems, *CMES: Computer Modeling in Engineering & Sciences*, Vol. 10, No. 1, pp. 13-38.

Divo E., Kassab A.J. (2005): Transient non-linear heat Conduction Solution by a Dual Reciprocity Boundary Element Method with an effective posteriori error estimator, *CMC: Computers, Materials, & Continua*, Vol. 2, No. 4, pp. 277-288.

Grysa K. (1989): On the exact and approximate methods of solving inverse problems of temperature fields. Rozprawy, *Politechnika Poznańska*, 204, Poznań(in Polish).

Hensel E.C., and Hills R.G. (1984): A space marching finite difference algorithm for the one dimensional inverse conduction heat transfer problem, *ASME paper*, No. 84-HT-48.

Hensel E.C., and Hills R.G., (1986): An initial value approach to the inverse heat conduction problem, *Trans. AMSE, J. Heat Transfer*, vol. 108, pp. 248-256.

Hills R.G., and Hensel E.C. (1986): One-dimensional nonlinear inverse heat conduciton technique, *Numerical Heat Transfer*, vol. 10, pp. 369-393.

Hore P.S., Kruttz G.W., and Schoenhals R.J. (1977): Application of the finite element method to the inverse heat conduction problem, *ASME paper*, NO. 77-WA/TM-4.

Imber M., and Khan J. (1972): Prediction of transient temperature distributions with embedded thermocouples, *AIAA Journal*, vol. 10, pp. 784-789.

Ling X., Keanini R.G., and Cherukuri H.P. (2003): A noniterative finite element method for inverse heat conduction problems, *Int. J. Numerical Method in Engineering*, vol. 56, pp. 1315-1334.

Ling X., Cherukuri H.P., and Keanini R.G. (2005): A modified sequential function specification finite element-based method for parabolic inverse heat conduction problems, *Comp. Mechanics*, vol. 36, pp. 117-128.

Ling X., Cherukuri H.P., and Horstemeyer M.F. (2006): A hybrid regularization method for inverse heat conduction problems, *Int. J. Numer. Methods Engng.*, vol. 65, pp. 2246-2264.

Maciag A., Al-Khatib J.M. (2000): Stability of solutions of the overdetermined inverse heat conduciton problems when descretized with respect to time, *Int. J. Numer. Methods for Heat & Fliud Flow*, vol. 10, pp. 228-244.

Murio D.A. (1993): The mollification method and the numerical solution of ill-posed problems, New York, Wiley.

Özisik M.N., and Orlande H.R.B. (2000): Inverse Heat Transfer, Taylor-Francis, New York.

Sladek J., Sladek V., Atluri S.N. (2004): Meshless local Petrov-Galerkin method for heat conduction problem in an anisotropic medium, *CMES: Computer Modeling in Engineering & Sciences*, Vol. 6, No. 3, pp. 309-318.

Sparrow E.M., Haji-Sheikh A., and Lundgren T.S. (1964): The inverse problem in transient heat conduction, *ASME J. of Applied Mechanics*, vol. 86, pp. 369-375.

Stolz Jr. G. (1960): Numerical solutions to an inverse problem of heat conduction for simple shapes, *J. Heat Transfer, Trans. ASME*, vol. 82, pp. 20-26.

Taler J. (1996): A semi-numerical method for solving inverse heat conduction problems, *Heat and Mass Transfer*, vol. 31, pp. 105-111.

Tandy D.F., Trujillo D.M., and Busby H.R. (1986): Solution of inverse heat conduction problems using an eigenvalue reduction technique,*Numerical Heat Transfer*, vol. 10, pp. 597-617.

Tikhonov A.N., and Arsenin V.Y. (1977): Solution of ill-posed problems, Winston & Sons, Wnashington, DC.

Trujillo D.M., and Busby H.R. (1997): Practical inverse analysis in engineering, CRC Press, New York.

Weber C.F. (1981): Analysis of the ill-posed inverse heat conduction problem, *Int. J. Heat Mass Transfer*, vol. 24, pp. 1783-1792.